International Journal of Heat and Mass Transfer 201 (2023) 123673

Contents lists available at ScienceDirect

International Journal of Heat and Mass Transfer

journal homepage: www.elsevier.com/locate/hmt

Tuning thermal transport across monolayer MoS_2/Si heterostructure via substrate nanogrooving

Wenxiang Liu[a], Xiaona Huang[a,*], Yanan Yue[a,b,*]

[a] School of Power and Mechanical Engineering, Wuhan University, Wuhan, Hubei 430072, China
[b] Department of Mechanical and Manufacturing Engineering, Miami University, Oxford, OH 45056, United States

ARTICLE INFO

Article history:
Received 24 August 2022
Revised 21 October 2022
Accepted 14 November 2022

Keywords:
MoS_2-Si heterostructure
Surface topography modification
Thermal properties regulation

ABSTRACT

Substrate-supported two-dimensional (2D) material heterostructures have been widely applied in electronic and photonic devices. However, the substrate reduces the original high thermal conductivity of 2D materials and limits the heat dissipation due to the interface thermal resistance. Here, the effects of the substrate surface topography on the thermal transport properties of the MoS_2-Si heterostructure are investigated via molecular dynamics simulations. The decreased in-plane thermal conductivity of the monolayer MoS_2 and surprisingly enhanced interface thermal transport of the MoS_2-Si heterostructure are found by introducing the shallow nanogroove on the substrate surface. The results are ascribed to the morphology change of the supported MoS_2, which bends to fit the substrate surface topography due to the van der Waals force at the small groove depth. In addition, the force weakens and the supported MoS_2 restores to flat with the increase of groove depth, resulting in higher in-plane thermal conductivity and thermal resistance compared to those without grooves, which is due to the disappearance of the substrate effect in the nanogroove area. This work elucidates the fundamental understanding of heat transfer in heterostructures. It provides new insights to enhance the heat dissipation in electronic devices by introducing nanoscale roughness.

1. Introduction

Nanotechnology and materials science advancements have resulted in novel two-dimensional (2D) materials, like graphene [1], MoS_2 [2], and *h*-BN [3]. Thermal transport in those 2D materials was a fascinating field where discoveries are constantly being made over the past two decades [4–6]. Abnormal high thermal conductivity was found in two-dimensional materials, which makes them the promising materials to confront the ever-increasing challenges in the electronic device thermal management [7,8]. However, in the realistic development and application of 2D materials, the substrate is typically an integral part since most 2D materials are grown on them or placed on metal and insulator substrates in many cases [9], which inevitably modifies and tunes the intrinsic thermal properties of 2D materials [10]. At the same time, the high thermal resistance in the 2D materials-substrate interface also limited the heat dissipation. Hence, a thorough understanding of the substrate effects and finding a way to enhance the thermal transport in 2D materials-substrate is urgent to the application of 2D materials and thermal management.

The significant development in experimental measurement and theoretical calculations have been achieved [11] along with the discovery and understanding that the thermal properties of supported 2D materials are quite different from the suspended ones [12]. Seol et al. [13] found that the thermal conductivity of silicon dioxide supported graphene reduces to 600 W/m K, although the thermal conductivity of graphene is approximately 3000–5000 W/m K. This reduction is ascribed to the leaking phonon to the substrate and the strong interface phonon scattering. Chen et al. [14] compared the in-plane thermal conductivity of suspended graphene and SiO_2 substrate supported graphene via molecular dynamics simulations and found a reduction of about 40% in the supported one. They further found that flexural acoustic (ZA) phonon shifts to the high frequency after supported by the substrate using spectral energy density analysis. The scattering of ZA phonon leads to the reduction of in-plane thermal conductivity, which widely appears in other 2D material-substate systems, for example, MoS_2-SiO_2 [15] and silicene-amorphous SiO_2 systems [16]. Furthermore, interface thermal resistance caused by the interface's presence in those systems also attracts much attention [17]. A comprehensive study of the

* Corresponding authors at: School of Power and Mechanical Engineering, Wuhan University, Wuhan, Hubei 430072, China.
E-mail addresses: xnhuang@whu.edu.cn (X. Huang), yyue@whu.edu.cn (Y. Yue).

https://doi.org/10.1016/j.ijheatmasstransfer.2022.123673
0017-9310/

interface thermal resistance with various substrates (e.g., GaN, diamond, silicon carbide, silicon, and sapphire) indicated that interface thermal resistance is changed with substrate type [18], which varies at the range of 10~60 m^2 K/GW, and diamond provides the minimum thermal resistance. Farahani et al. [19] found that the thermal resistances of MoS_2 on crystalline and amorphous silica substrates are close, and there is a slight difference for the systems with different MoS_2 layer numbers.

Such understandings led to another interesting tropic-thermal transport enhancement in 2D materials-substrate heterostructure. By tuning the interface van der Waals (vdw) force binding energy, zhang et al. [20] optimized the overall heat transfer of MoS_2-α-SiO_2 heterostructure. They found that the thermal conductivity decreases with the increase of the binding energy, while the interface thermal transport is enhanced. In addition, layer number plays another key role in lightening the effects of substrate [21]. With the increase of layer number, the thermal conductivity of 2D materials drops smaller than that of a single layer. Roughness, although as a controversial factor, is the simple and obvious way among many possibilities that could enhance the heat transfer. A considerable number of experiments and theoretical calculations [22,23] have been made to investigate the effects of roughness on heat transfer. Su et al. [24] measured the thermal resistance between aluminum nitride (AlN) thin films and SiC. An order-of-magnitude larger thermal boundary resistance was measured with the increased surface roughness supports that roughness further hinders the interface thermal transport. However, some others simulations [25,26] suppose that nm-roughness will enhance the interface thermal transport. The opposing finding inspired us to systematically study the roughness effect on in-plane thermal conductivity and interface thermal transport of the substrate-supported 2D material systems.

Here, the thermal transport through MoS_2-Si heterostructure is comprehensively investigated, and importantly, the influences of nanoscale roughness are analyzed. The framework of this paper is as follows. Section two introduces the methods for calculating the thermal conductivity and interface thermal resistance. Section three presents the results of the effects of nanoscale roughness on the thermal conductivity and interface thermal resistance, showing an exception of the interface thermal transport enhancement when the roughness is small and the increased thermal conductivity at the large roughness.

2. Models and simulation approach

All simulations are performed using the large scale atomic/molecular massively parallel simulator [27] (LAMMPS). The free and periodic boundary conditions are applied to the out-of-plane (z) direction and in-plane (x and y) direction, respectively. Stilling-Weber potentials developed from Kandemir et al. [28] and Stillinger and Weber [29] are used to model the interactions in MoS_2 and Si, which are expressed as:

$$E = \sum_i \sum_{j>i} \phi_2(r_{ij}) + \sum_i \sum_{j\neq i} \sum_{k>j} \phi_3(r_{ij}, r_{ik}, \theta_{ijk}) \quad (1)$$

where ϕ_2 and ϕ_3 are two-body and three-body interactions, respectively. Lennard-Jones (LJ) potentials are employed to describe the interlayer force between the monolayer MoS_2 and Si substrate, which can be written as:

$$V(r) = 4\chi\varepsilon\left[\left(\frac{\sigma}{r}\right)^{12} - \left(\frac{\sigma}{r}\right)^{6}\right] \quad (2)$$

where ε is the potential well depth and σ is distance parameters, which are summarized in Table 1 [19]. The timestep and cut-off distance are set as 0.5 fs and 12.5 Å, separately. To build the initial configuration of MoS_2-Si heterostructure, 30 × 10 unit cells for MoS_2 and 30 × 6 unit cells for Si are chosen to minimize the lattice mismatch. Hence, the final in-plane simulation areas are 16.65 × 3.17 nm^2 and the lattice mismatch between supported MoS_2 and substrate Si was less than 3%. Meanwhile, a vacuum layer of 2 nm thickness was added along the out-of-plane direction and the thicknesses of the MoS_2 monolayer and Si substrate are 6.15 Å [30] and 4.26 nm, respectively, with their distance of approximately 3 Å [15]. Finally, a constant width and changed depth nanogroove is dug at the middle of substrate. The whole system is relaxed under the canonical ensemble to obtain a more stable configuration.

Table 1
The LJ parameters, including energy parameters (ε) and distance parameters (σ) between MoS_2 and Si.

	ε (eV)	σ (Å)
Si-Mo	0.00562	3.27
Si-S	0.01242	3.71

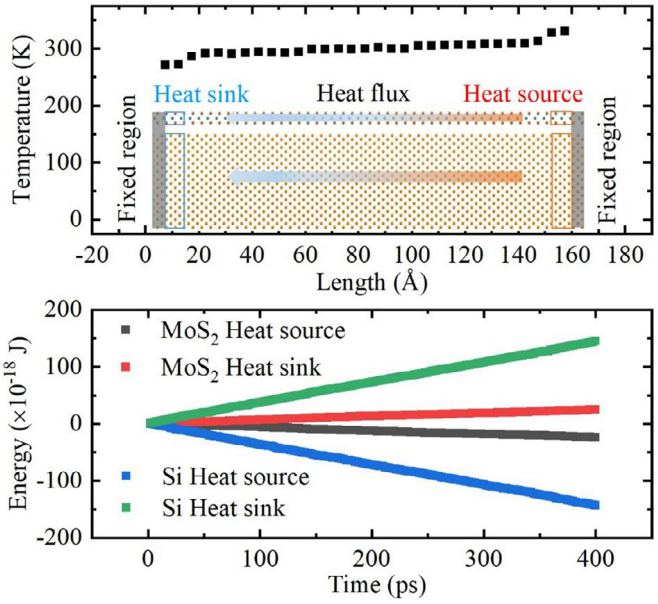

Fig. 1. Illustration of NEMD simulations: (a) NEMD setup for MoS_2-Si heterostructure and the typical temperature profile of MoS_2. (b) Exchanged energy of heat source and heat sink over time.

The nonequilibrium molecular dynamics (NEMD) and pump-probe transient thermoreflectance methods are used to investigate the in-plane and interface thermal transport of the heterostructure. In NEMD simulations, the keystone is to establish a stable temperature gradient, then the thermal conductivity is calculated based on Fourier's law.

$$k = -\frac{dQ/dt}{dT/dx} \quad (3)$$

where k is the thermal conductivity; dQ/dt represents the energy exchange rate; dT/dx is the temperature gradient. In NEMD simulations, the heterostructure is firstly relaxed under the canonical ensemble (NVT) at 300 K for 400 ps with the temperature controlled by Nosé–Hoover thermostat. Then, another 50 ps micro-canonical ensemble (NVE) is applied to check the energy conservation and temperature equilibrium. Four heat baths controlled by Langevin thermostat are used for supported MoS_2 and substrate Si, as shown in Fig. 1. The heat baths at each end are set as 330 K and 270 K, respectively. After that, the simulations were run for 1.5 ns with 1 ns used to reach the new equilibrium state and another 0.5 ns to collect the temperature distribution and energy change. Fig. 1(a) shows the final averaged temperature profile, and the energy change varies with time is plotted in Fig. 1(b). The tempera-

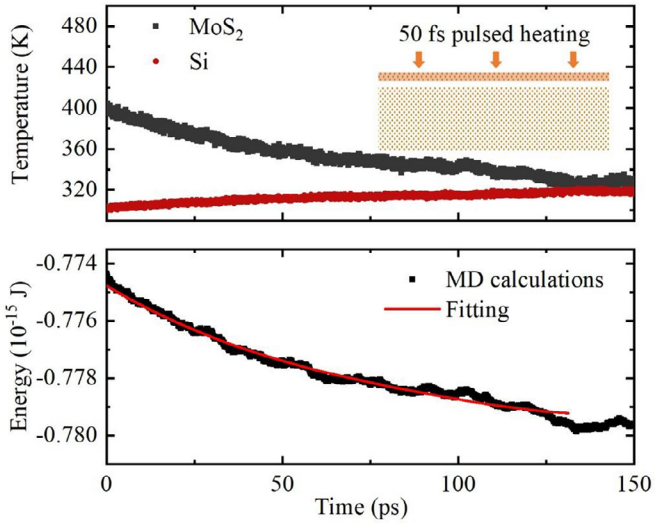

Fig. 2. (a) The history of the MoS_2 and Si temperature change. (b) Energy recording and energy fitting of the supported MoS_2 for interface thermal resistance calculations.

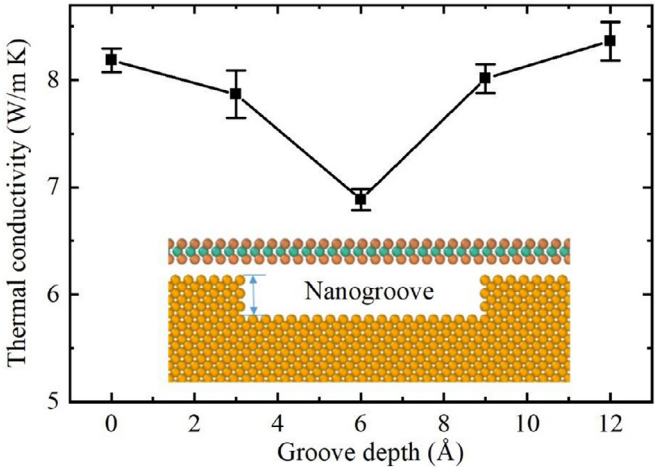

Fig. 3. Thermal conductivity of MoS_2 variations with groove depth (d). A typical atomic configuration of the MoS_2-Si heterostructure with nanogroove.

ture profile includes two parts, i.e., the nonlinearity near the heat bath and the line region away from the heat bath. We obtain the temperature gradient directly from the division of the temperature difference between the two heat baths and the length of the supported MoS_2, as Li et al suggested [31]. In addition, the heat flux can be calculated from the gradient of the energy profile. The energy changes of hot slab and cold slab are symmetry which certifies the constant of the temperature gradient. Finally, the thermal conductivity is easily acquired based on the above Fourier's law.

The pump-probe transient thermoreflectance method is an optical technique widely used to measure the thermal resistance across the material interface [23,32,33]. The method is used here by MD simulation to calculate the thermal resistance between the supported MoS_2 and Si substrate. The simulation process is similar to the experimental measurements. An extremely short heat impulse is imposed on the suspended MoS_2 (Fig. 2(a)), and the atomic velocities of suspended MoS_2 are rescaled, resulting in a sharp temperature increase. The MoS_2 temperature gradually decreases due to the heat transfer to the substrate after the excitation. The temperature and energy changes with time are recorded in this process, and the thermal resistance can be calculated based on the following equation:

$$\frac{\partial E_t}{\partial t} = \frac{T_{MoS_2} - T_{Si}}{R/A} \tag{4}$$

where E_t is the MoS_2 energy at time t; T_{MoS2} ad T_{Si} are the temperatures of the supported MoS_2 and Si substrate, respectively; R is the thermal resistance; A represents the cross area. However, the calculated thermal resistance based on the Eq. (4) makes a large uncertainty subject to the energy decay noise. Hence, an integral form (Eq. (5)) is applied to reduce this uncertainty and obtain more accurate results.

$$E_t = E_0 + (R/A)\int_0^t (T_{MoS_2} - T_{Si})dt \tag{5}$$

In this method, the heterostructure is first relaxed under the canonical ensemble and microcanonical ensemble sequentially at 300 K. Then, a 1.49×10^{-4} W thermal impulse is applied to the suspended MoS_2 for 50 fs. After the excitation, the temperature of the suspended MoS_2 increases to 404 K. Meanwhile, the temperature of the adjacent Si surface maintains at the initial temperature. Subsequently, temperature and energy changes over time are recorded for 250 ps, and each data point is averaged over 100 time steps to reduce data noise. The final results are illustrated in Fig. 2. The temperature and energy of the suspended MoS_2 dramatically decrease before 50 ps due to the strong heat transfer caused by the large temperature differences. At the same time, a slight temperature augment in the substrate is observed. The fitted line based on Eq. (5) (the red line in Fig. 2b) is well matched with the energy decay line, which validates this approach for interface thermal resistance extractions.

3. Results and discussion

3.1. Effect of nanogroove on in-plane thermal transfer

Substrates roughness is considered by inducing a nanogroove with constant width and depths ranging from 0 ~ 1.2 nm. Although there are millions of roughness patterns [34], only the rectangular-shaped nanogrooves are engraved to simplify the model establishment. The calculated in-plane thermal conductivities of the monolayer MoS_2 are illustrated in Fig. 3. The thermal conductivity of the supported MoS_2 on Si substrate without nanogroove is 8.18 W/m K. In addition, the thermal conductivity of suspended monolayer MoS_2 with the same size as the substrate supported MoS_2 is calculated to be approximately 9.47 W/m·K, which is consistent with the previous studies of suspended MoS_2 [30,35,36]. It is worth mentioning that the thermal conductivity of suspended monolayer MoS_2 is slightly higher than that of substrate supported MoS_2, and this phenomenon has widely appeared in other 2D materials [14,37,38]. Theoretical research ascribes this reduction to the phonon scattering with the substrate [14]. With the increase of d from 0 to 0.6 nm, the in-plane thermal conductivity decreases from 8.18 W/m K to the minimum (6.88 W/m K), showing a 16% reduction. Then the thermal conductivity rises with d when d transcends 0.6 nm. Finally, the thermal conductivity is higher than that without nanogroove when d reaches 1.2 nm.

To understand the nanogroove depth dependent in-plane thermal conductivity in the supported MoS_2, the atomic configurations are analyzed to show its change with the nanogroove depth. The supported MoS_2 is bent to fit the substrate structure with a relatively shallow nanogroove, as shown in Fig. 4. However, the monolayer MoS_2 keeps flat when the nanogroove is deep enough. To characterize this bend degree, the ensemble-averaged bend is calculated as the following equation:

$$D = \left\langle \sqrt{\sum_i^N (z_i - \bar{z})^2 / N} \right\rangle \tag{6}$$

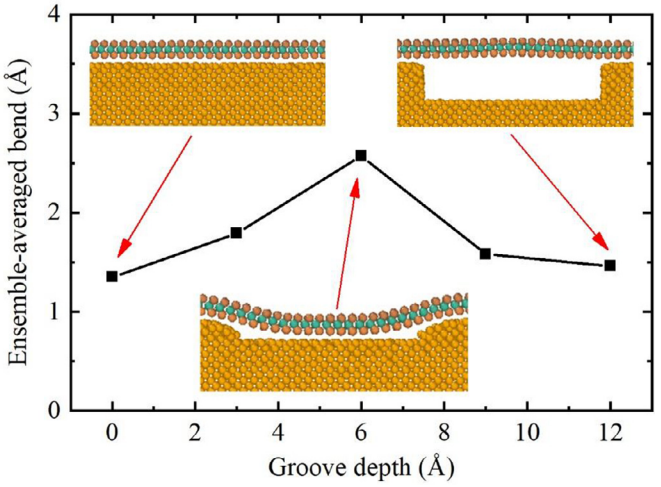

Fig. 4. Ensemble-averaged bend variations with d. The final atomic configuration of balanced system when d equals to 0, 0.6 and 1.2 nm.

where z_i is the z coordinate of atom i, and $\bar{z}$ means the averaged z coordinate of all atoms. Fig. 4 shows the bend degrees of the monolayer MoS_2 at different nanogroove depths. The ensemble-averaged bend increases with d until it reaches 0.6 nm, then decreases to the value close to that without nanogrooves. Bending curvature strongly influences the in-plane thermal conductivity, which was also reported by Liu and Xu [39]. Similar to our results, the thermal conductivity monotonously decreases with the rise of bending curvature. The reasons are ascribed in several respects. To commence, the presence of bending results in the flattening of ZA mode and strong phonon localization. In addition, especially in small sizes, the bending will lead to phonon hybridization, which strengthens the phonon energy dissipation. All of those effects contribute to the weakness of in-plane thermal transport.

The supported MoS_2 right over the nanogroove regions is bent to close contact with the substrate due to their interlayer force when d reaches 0.6 nm, which induces strong strain within the monolayer MoS_2. The induced strain leads to the decreased thermal conductivity of the supported MoS_2, which has been certified in previous works [40–42]. In addition, the final steady configuration of the supported MoS_2 is the combined action of two forces, i.e., tensile stress and interlayer interaction. The interlayer vdw force weakens and leads to stress reduction when d continues increase, resulting in the supported MoS_2 flattened when d is sufficiently large, as the interlayer interactions are weakened enough. Thus, the in-plane thermal transport is reinforced. Meanwhile, the disappearance of the substrate effect in the nanogroove area also facilitates the in-plane thermal transport, which makes the thermal conductivity even larger than that without nanogrooves.

The phonon density of states (PDOS) is calculated to reveal the phonon transport mechanisms of the monolayer MoS_2, as shown in Fig. 5(a, b). PDOS can be calculated based on the Fourier transform of the velocity autocorrelation function, which is expressed as:

$$F(\omega) = \frac{1}{\sqrt{2\pi}} \int_{-\infty}^{+\infty} \frac{\langle v(0) \cdot v(t) \rangle}{\langle v(0) \cdot v(0) \rangle} e^{i\omega t} dt \tag{7}$$

where v is the atomic velocity, and the angle brackets represent the ensemble average. A large $F(\omega)$ means more phonons are occupied at the given frequency. The in-plane and out-of-plane PDOS of the supported MoS_2 when d equals 0 and 0.6 nm are depicted in Fig. 5(a, b). The PDOS is consistent with the previous calculation with the same peak position and max frequency [43]. Meanwhile it shows that the in-plane modes (vibrations along the x and y directions) undergo a softening with a lower peak after the

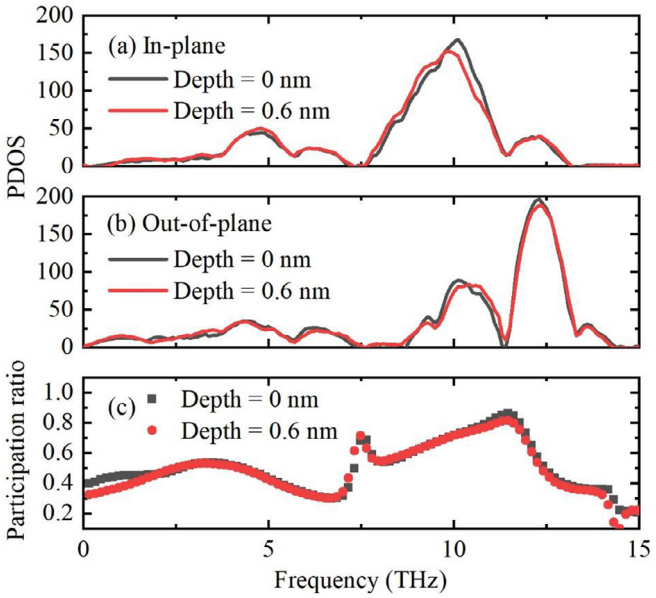

Fig. 5. (a) In-plane and (b) out-of-plane phonon density of state of the supported MoS_2. (c) Participation ratio of the supported MoS_2 for d equals to 0 and 0.6 nm.

nanogrooves are induced, whereas the out-of-plane flexural mode (z-direction) is slightly blue-shifted. This phenomenon is also observed in works focused on manipulating the thermal conductivity of monolayer MoS_2 by changing strain [40,43], which suggests the correctness of the above explanation. In addition, the participation ratio (PR) can provide information about each phonon mode and describe the spatial localization. PR is defined for each eigenmode λ as:

$$P_\lambda^{-1} = N \sum_i \left(\sum_\alpha \varepsilon_{i\alpha,\lambda}^* \varepsilon_{i\alpha,\lambda} \right)^2 \tag{8}$$

where $\varepsilon_{i\alpha,\lambda}$ is the α^{th} eigenvector component of eigenmodel λ for the i^{th} atom. If all atoms participate in a specific phonon mode, this mode can diffuse to the entire space, and the corresponding PR value equals 1. However, if only small numbers of atoms are attributed to the mode, the mode is localized. The smaller value of PR represents the more intense phonon localization. Fig. 5(c) compares the PR of the supported MoS_2 when d equals 0 and 0.6 nm. Below 2.5 THz and between the high frequency of 10–15 THz, PR decreases with the increase of d, representing that more phonons are localized, leading to a decrease in thermal conductivity.

3.2. Effect of nanogroove on interface thermal resistance

The interface thermal resistance between the monolayer MoS_2 and substrate Si is investigated, as shown in Fig. 6. Surprisingly, the thermal resistance firstly decreases from 6.38×10^{-8} to 4.46×10^{-8} K m^2/W with the d increasing from 0 to 0.6 nm, nearly a 29% drop, and subsequently increases to 8×10^{-8} K m^2/W, followed by a sudden and sharp decrease to 6.59×10^{-8} K m^2/W, which is higher than that without nanogrooves. This phenomenon has been observed in graphene nanoribbon-Cu heterostructure [26] and graphene nanoribbon-Si heterostructure [25]. However, more substantial thermal resistance reduction was found due to a larger width and a shallower depth used in our study compared to those systems. Our results demonstrate that a rough surface does not always impede the heat transport at the interface but may enhance it.

To explore the mechanisms behind the interface thermal transport enhancement, forces are firstly considered. Based on the

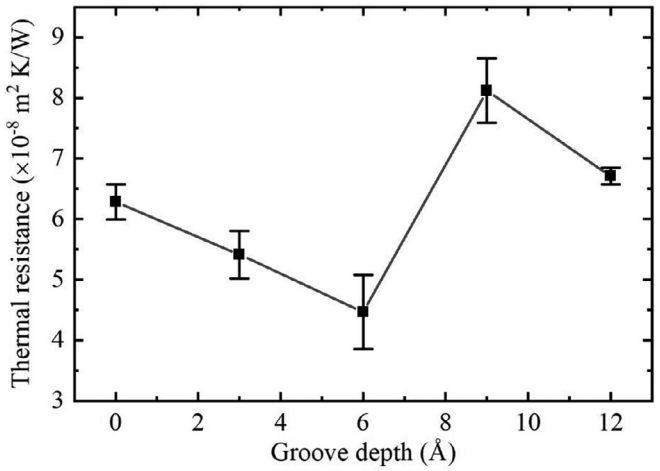

Fig. 6. Interface thermal resistance change with groove depth.

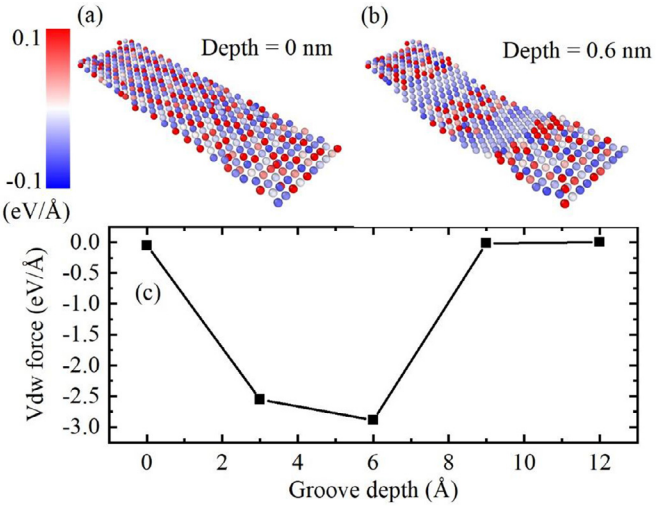

Fig. 7. Atomic vdw force distribution of (a) $d = 0$ nm and (b) $d = 0.6$ nm. (c) Overall vdw force in nanogroove region variations with d.

above analysis of thermal conductivity, the final stable configuration is balanced under two forces of in-plane tensile stress and interlayer vdw force, which also play the determining factors in interface thermal transport. Fig. 7(a) and (b) depict the atomic force of the substrate on the supported MoS_2 without nanogroove and with a 0.6 nm depth nanogroove, respectively. The force of the substrate on the nearest MoS_2 layer is analyzed, and the atom force on farther atoms in MoS_2 can be neglected. The red color denotes repulsive force, and the blue color represents attractive force. The repulsive and attractive force is evenly distributed in the flat monolayer MoS_2 but is uneven in the bent one, especially near the nanogroove edge, where exits strong attractive force. Fig. 7(c) illustrates the evolution of the total vdw force on the MoS_2 directly above the nanogroove region with the nanogroove depth. The attractive force increases with the depth when the depth smaller than 0.6 nm. The whole structure maintains the equilibrium state, so the overall force of the supported MoS_2 is balanced and approximated as zero. The bent MoS_2 and the substrate show strong attractive force when d is small. Thus, the averaged net repulsive force arises in the supported area since the overall force of monolayer MoS_2 is zero. The enhanced local stress in the supported area enhances the heat transport at the interface [44,].

In addition, the supported MoS_2 is no longer bent to fit the substrate, and separation occurs when the nanogroove deeps enough.

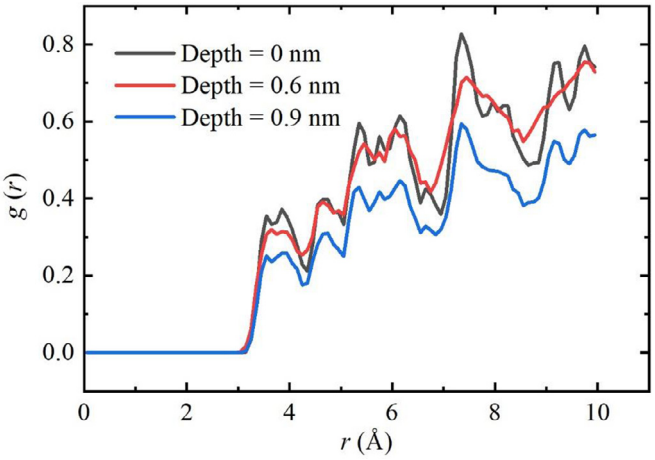

Fig. 8. Radial distribution function $g(r)$ between the MoS_2 of the layer closest to the substrate and substrate Si for different d.

Meanwhile, the overall vdw force in the nanogroove region eventually decreased to zero (Fig. 7(c)), which corresponds to the increase in interface thermal resistance (Fig. 6). To further explain the sudden increase in thermal resistance at a depth of 0.9 nm, the radial distribution function (RDF) $g(r)$ between the atomic layer of MoS_2 closest to the substrate and the Si substrate is calculated and illustrated in Fig. 8. The black, red, and blue lines represent the RDF at d equals 0, 0.6, and 0.9 nm, respectively. It can be found that the $g(r)$ values of black line and red line are similar, which indicates that the supported MoS_2 bends to fit the substrate surface at the nanogroove depth of 0.6 nm. A large gap exists between the red line and the blue line, indicating that the separation occurs and fewer atoms are involved in heat transport leading to the increased interface thermal resistance at d equals 0.9 nm. Meanwhile, the bending tensile stress is also considered as another impeding factor to hinder the interface thermal transport, which has been reported in past works [11,45]. The existence of tensile stress further increases the interface thermal resistance at d equals 0.9 nm. Subsequently, with the increase of d, the tensile stress slowly disappears as the flattening of the supported MoS_2, leading to the enhancement of interface thermal transport and reduction of the interface thermal resistance.

4. Conclusion

In summary, the roughness effects on heat transfer through the MoS_2-Si heterostructure are systematically investigated at the atomic scale. The thermal conductivity of the supported MoS_2 and the interface thermal resistance of the MoS_2-Si heterostructure are calculated via molecular dynamics simulations. The thermal conductivity shows a trend of decline first and then increases with the nanogroove depth. The calculated ensemble-averaged bend from atomic configuration shows that the tensile strain plays the dominant role in reducing the thermal conductivity after introducing the shallow nanogrooves. The PDOS and PR of the supported MoS_2 further explained the phenomenon. The increase in thermal conductivity when d is larger than 0.6 nm is attributed to the less effect of the substrate. The thermal conductivity at nanogroove depth of 1.2 nm is higher than that without nanogrooves due to the disappearance of the substrate effect in the nanogroove area. In addition, the interface thermal transport is surprisingly enhanced when introducing a 0.6 nm depth nanogroove due to the uneven press distribution, which is supported by the calculated interlayer vdW forces. Subsequently, the interface thermal resistance increases with the nanogroove depth when the depth is larger than

0.6 nm, indicating that the interface thermal transport is weakened. Our study provides insights into the thermal properties of the MoS_2-Si heterostructure and proves that the thermal properties can be optimized via nanoengineering.

Declaration of Competing Interest

The authors declare that they have no known competing financial interests or personal relationships that could have appeared to influence the work reported in this paper.

CRediT authorship contribution statement

Wenxiang Liu: Methodology, Validation, Visualization, Investigation, Formal analysis, Writing – original draft, Writing – review & editing. **Xiaona Huang:** Funding acquisition, Formal analysis, Writing – original draft, Writing – review & editing. **Yanan Yue:** Funding acquisition, Conceptualization, Supervision, Writing – review & editing.

Data Availability

Data will be made available on request.

Acknowledgment

This study was supported by the financial support from the National Key Research and Development Program of China (No. 2019YFE0119900), National Natural Science Foundation of China (No. 52076156), Natural Science Foundation of Hubei Province (No. 2021CFB120), and Fundamental Research Funds for the Central Universities (No. 2042022kf1020). The authors appreciate the support from the Supercomputing Center of Wuhan University.

Reference

[1] C.H. Lui, L. Liu, K.F. Mak, G.W. Flynn, T.F. Heinz, Ultraflat graphene, Nature 462 (7271) (2009) 339–341.
[2] K.K. Liu, W.J. Zhang, Y.H. Lee, Y.C. Lin, M.T. Chang, C. Su, C.S. Chang, H. Li, Y.M. Shi, H. Zhang, C.S. Lai, L.J. Li, Growth of large-area and highly crystalline MoS_2 thin layers on insulating substrates, Nano Lett. 12 (3) (2012) 1538–1544.
[3] M. Morscher, M. Corso, T. Greber, J. Osterwalder, Formation of single layer h-BN on Pd(111), Surf. Sci. 600 (16) (2006) 3280–3284.
[4] Z.W. Zhang, Y.L. Ouyang, Y. Cheng, J. Chen, N.B. Li, G. Zhang, Size-dependent phononic thermal transport in low-dimensional nanomaterials, Phys. Rep. 860 (2020) 1–26.
[5] N.A. Roberts, D.G. Walker, A review of thermal rectification observations and models in solid materials, Int. J. Therm. Sci. 50 (5) (2011) 648–662.
[6] K. Kanahashi, J. Pu, T. Takenobu, 2D materials for large-area flexible thermoelectric devices, Adv. Energy Mater. 10 (11) (2020) 1902842.
[7] S. Ghosh, I. Calizo, D. Teweldebrhan, E.P. Pokatilov, D.L. Nika, A.A. Balandin, W. Bao, F. Miao, C.N. Lau, Extremely high thermal conductivity of graphene: prospects for thermal management applications in nanoelectronic circuits, Appl. Phys. Lett. 92 (15) (2008) 151911.
[8] H.F. Song, J.M. Liu, B.L. Liu, J.Q. Wu, H.M. Cheng, F.Y. Kang, Two-dimensional materials for thermal management applications, Joule 2 (3) (2018) 442–463.
[9] G. Iannaccone, F. Bonaccorso, L. Colombo, G. Fiori, Quantum engineering of transistors based on 2D materials heterostructures, Nat. Nanotechnol. 13 (3) (2018) 183–191.
[10] S.H. Bae, H. Kum, W. Kong, Y. Kim, C. Choi, B. Lee, P. Lin, Y. Park, J. Kim, Integration of bulk materials with two-dimensional materials for physical coupling and applications, Nat. Mater. 18 (6) (2019) 550–560.
[11] Y.N. Yue, J.C. Zhang, X.W. Wang, Micro/nanoscale Spatial Resolution Temperature Probing for Interfacial Thermal Characterization of Epitaxial Graphene on 4H-SiC, Small 23 (7) (2011) 3324–3333.
[12] Q.Y. Li, K.L. Xia, J. Zhang, Y.Y. Zhang, Q.Y. Li, K. Takahashi, X. Zhang, Measurement of specific heat and thermal conductivity of supported and suspended graphene by a comprehensive Raman optothermal method, Nanoscale 9 (30) (2017) 10784–10793.
[13] J.H. Seol, I. Jo, A.L. Moore, L. Lindsay, Z.H. Aitken, M.T. Pettes, X.S. Li, Z. Yao, R. Huang, D. Broido, N. Mingo, R.S. Ruoff, L. Shi, Two-dimensional phonon transport in supported graphene, Science 328 (5975) (2010) 213–216.
[14] J. Chen, G. Zhang, B.W. Li, Substrate coupling suppresses size dependence of thermal conductivity in supported graphene, Nanoscale 5 (2) (2013) 532–536.
[15] A.J. Gabourie, S.V. Suryavanshi, A.B. Farimani, E. Pop, Reduced thermal conductivity of supported and encased monolayer and bilayer MoS_2, 2D Mater. 8 (1) (2020) 011001.
[16] Z. Wang, T. Feng, X. Ruan, Thermal conductivity and spectral phonon properties of freestanding and supported silicene, J. Appl.Phys. 117 (8) (2015) 084317.
[17] S. Sudhakar, J.A. Weibel, F. Zhou, E.M. Dede, S.V. Garimella, Area-scalable high--heat-flux dissipation at low thermal resistance using a capillary-fed two-layer evaporator wick, Int. J. Heat Mass Trans. 135 (2019) 1346–1356.
[18] K. Park, C. Bayram, Thermal resistance optimization of GaN/substrate stacks considering thermal boundary resistance and temperature-dependent thermal conductivity, Appl. Phys. Lett. 109 (15) (2016) 151904.
[19] H. Farahani, A. Rajabpour, M. Khanaki, A. Reyhani, Interfacial thermal resistance between few-layer MoS_2 and silica substrates: a molecular dynamics study, Comput. Mater. Sci. 142 (2018) 1–6.
[20] L. Zhang, Y. Zhong, X. Qian, Q. Song, J. Zhou, L. Li, L. Guo, G. Chen, E.N. Wang, Toward optimal heat transfer of 2D–3D heterostructures via van der waals binding effects, ACS Appl. Mater. Interfaces 13 (38) (2021) 46055–46064.
[21] A.L. Moore, L. Shi, Emerging challenges and materials for thermal management of electronics, Mater. Today 17 (4) (2014) 163–174.
[22] Z. Liang, K. Sasikumar, P. Keblinski, Thermal transport across a substrate-thin–film interface: effects of film thickness and surface roughness, Phys. Rev. Lett. 113 (6) (2014) 065901.
[23] J.Z Zhang, Y Hong, Y.N. Yue, Thermal Transport across Graphene and Single Layer Hexagonal Boron Nitride, J. Appl. Phys. 117 (13) (2015) 134307.
[24] Z.H. Su, J.P. Freedman, J.H. Leach, E.A. Preble, R.F. Davis, J.A. Malen, The impact of film thickness and substrate surface roughness on the thermal resistance of aluminum nitride nucleation layers, J. Appl. Phys. 113 (21) (2013) 213502.
[25] J.C. Zhang, Y.C. Wang, X.W. Wang, Rough contact is not always bad for interfacial energy coupling, Nanoscale 5 (23) (2013) 11598–11603.
[26] Y. Hong, L. Li, X.C. Zeng, J. Zhang, Tuning thermal contact conductance at graphene-copper interface via surface nanoengineering, Nanoscale 7 (14) (2015) 6286–6294.
[27] S. plimpion, Fast parallel algorithms for short-range molecular dynamics, J. Comput. Phys. 117 (1995) 1–19.
[28] A. Kandemir, H. Yapicioglu, A. Kinaci, T. Cagin, C. Sevik, Thermal transport properties of MoS_2 and $MoSe_2$ monolayers, Nanotechnology 27 (5) (2016) 055703.
[29] F.H. Stillinger, T.A. Weber, Computer simulation of local order in condensed phases of silicon, Phys. Rev. B Condens. Matter 31 (8) (1985) 5262–5271.
[30] A. Krishnamoorthy, P. Rajak, P. Norouzzadeh, D.J. Singh, R.K. Kalia, A. Nakano, P. Vashishta, Thermal conductivity of MoS_2 monolayers from molecular dynamics simulations, AIP Adv. 9 (3) (2019) 035042.
[31] Z. Li, S.Y. Xiong, C. Sievers, Y. Hu, Z.Y. Fan, N. Wei, H. Bao, S.D. Chen, D. Donadio, T. Ala-Nissila, Influence of thermostatting on nonequilibrium molecular dynamics simulations of heat conduction in solids, J. Chem. Phys. 151 (23) (2019) 234105.
[32] H.D. Wang, W.G. Ma, Z.Y. Guo, X. Zhang, W. Wang, Measurements of electron—phonon coupling factor and interfacial thermal resistance of metallic nano-films using a transient thermoreflectance technique, Chin. Phys. B 20 (4) (2011) 040701.
[33] R.B. Wilson, B.A. Apgar, L.W. Martin, D.G. Cahill, Thermoreflectance of metal transducers for optical pump-probe studies of thermal properties, Opt. Express 20 (27) (2012) 28829–28838.
[34] Y.Q. Chen, Z.W. Shu, S. Zhang, P. Zeng, H.K. Liang, M.J. Zheng, H.G. Duan, Sub-10 nm fabrication: methods and applications, Int. J. Extreme Manuf. 3 (3) (2021) 032002.
[35] W. Li, J. Carrete, N. Mingo, Thermal conductivity and phonon linewidths of monolayer MoS_2 from first principles, Appl. Phys. Lett. 103 (25) (2013) 253103.
[36] X.K. Gu, B.W. Li, R.G. Yang, Layer thickness-dependent phonon properties and thermal conductivity of MoS_2, J. Appl. Phys. 119 (8) (2016) 085106.
[37] A. Rajabpour, S. Bazrafshan, S. Volz, Carbon-nitride 2D nanostructures: thermal conductivity and interfacial thermal conductance with the silica substrate, Phys. Chem. Chem. Phys. 21 (5) (2019) 2507–2512.
[38] L. Dong, X.S. Wu, Y. Hu, X.F. Xu, H. Bao, Suppressed thermal conductivity in polycrystalline gold nanofilm: the effect of grain boundary and substrate, Chin. Phys. Lett. 38 (2) (2021) 027202.
[39] Q.C. Liu, B.X. Xu, Anomalous thermal transport of mechanically bent graphene: implications for thermal management in flexible electronics, ACS Appl. Nano Mater. 5 (9) (2022) 13180–13186.
[40] Z.W. Ding, Q.X. Pei, J.W. Jiang, Y.W. Zhang, Manipulating the thermal conductivity of monolayer MoS_2 via lattice defect and strain engineering, J. Phys. Chem. C 119 (28) (2015) 16358–16365.
[41] L.Y. Zhu, T.T. Zhang, Z.M. Sun, J.H. Li, G.B. Chen, S.Y.A. Yang, Thermal conductivity of biaxial-strained MoS_2: sensitive strain dependence and size-dependent reduction rate, Nanotechnology 26 (46) (2015) 465707.
[42] Y. Gao, W.Z. Yang, B.X. Xu, Unusual thermal conductivity behavior of serpentine graphene nanoribbons under tensile strain, Carbon 96 (2016) 513–521.
[43] X.N. Wang, A. Tabarraei, Phonon thermal conductivity of monolayer MoS2, Appl. Phys. Lett. 108 (19) (2016) 191905.
[44] Y. Ueki, Y. Miyazaki, M. Shibahara, T. Ohara, Molecular dynamics study of thermal resistance of solid-liquid interface in contact with single layer of nanoparticles, Int. J. Heat Mass Trans. 120 (2018) 608–623.
[45] W.X. Liu, Y.Q. Wu, Y. Hong, B. Hou, J.C. Zhang, Y.N. Yue, Full-spectrum thermal analysis in twisted bilayer graphene, Phys. Chem. Chem. Phys. 23 (35) (2021) 19166–19172.